*M&C 2017 - International Conference on Mathematics & Computational Methods Applied to Nuclear Science & Engineering, Jeju, Korea, April 16-20, 2017, on USB (2017)*

# Calculation and Verification of Assembly Discontinuity Factors for the DRAGON/PARCS code sequence

Luca Liponi*, Julien Taforeau†, Alain Hébert*

*École Polytechnique de Montréal, Montréal, QC, Canada
†Institut de Radioprotection et de Sûreté Nucléaire (IRSN), PSN-EXP/SNC Fontenay-aux-Roses, 92262, France
luca.liponi@polymtl.ca, julien.taforeau@irsn.fr, alain.hébert@polymtl.ca

**Abstract** - *This paper is aimed at the implementation and validation of a calculation scheme between the lattice code DRAGON5 and the full-core simulation code PARCS. Following new developments in the framework DRAGON5-DONJON5, new possibilities are currently available to perform more accurate and faster neutronic deterministic simulations of Light Water Reactors (LWRs). An optimized single assembly 2-level scheme has recently been developed and has been proposed as a new standard for the generation of multi-parameter reactor database. At the same time, regarding full core simulation, the flexibility of the environment developed at École Polytechnique de Montréal (EPM) in collaboration with the Institut de Radioprotection et de Sûreté Nucléaire (IRSN), has demonstrated the straightforwardness of performing detailed core calculation with PARCS using a reactor database generator with DRAGON5-DONJON5. This work focuses on the comparison of different lattice calculations applied to the computational scheme DRAGON5-PARCS and its validation with a Monte Carlo calculation on a simplified PWR reactor problem. In particular, the validation tests were performed on a 3x3 cluster with three types of assemblies evaluated at zero burnup: UOX, UOX with AIC control rods and MOX. This study shows promising results for the calculation scheme, with accuracy in line with what has been already observed for single assembly homogenized parameters computed in infinite lattice approximation.*

## I. INTRODUCTION

Since 2012, the Institut de Radioprotection et de Sûreté Nucléaire (IRSN) has been working on a project called ORION dedicated to the optimization and improvement of computational tools and skills relative to neutronic deterministic simulations [1]. The aim is to have the tools currently in use for Light Water Reactors (LWR) to perform independent assessment regarding criticality safety and general reactor physics activities.

Given that a direct reactor simulation is not feasible due to the high complexity and time computation, a neutronic deterministic calculation is generally performed through two distinct and separate stages: assembly calculation, and full-core calculation. The focus of the ORION project is dedicated to these two stages of the reactor "calculation scheme". In this context the project is related to knowledge acquisition on criticality and reactor physics that can be adopted as new standards for IRSN safety assessment.

In order to find suitable software to work alongside the historical tools used at IRSN to perform complete reactor simulations, several options from different sources are currently in use and under analysis.

A central issue that must be taken into account in the implementation of a calculation scheme is the flux of information between the lattice and the core code. In fact, to be able to perform a full reactor calculation, a spatial homogenization of cross-sections needs to be considered at the end of the assembly calculation to generate the database of information required in the latter step. This database consists of macroscopic cross-sections and other homogenized parameters that describe the piecewise homogenized model of the complete reactor. It depends both on the homogenization technique and the format in which this information is stored.

The present work is dedicated to the implementation of the flux of information between the lattice code DRAGON5[2] and the full core simulation tool PARCS[3], and to perform diffusion calculation using the homogenized assembly parameters produced during the lattice calculation according to the General Equivalence Theory (GET)[4].

The coupling of DRAGON5-PARCS is an unique capability under development at IRSN to address reactor criticality and safety issues. DRAGON5 indeed is suited to perform the *superhomogénéisation* (SPH) equivalence technique[5], that includes the correction of the homogenized cross-sections directly inside the code after the transport calculation. However, currently, DRAGON5 is not able to generate the homogenized parameters required to implemenent direct use of the GET equivalence technique using Assembly Discontinuity Factor (ADF). In order to accomplish that, new tools and modification of DRAGON5 have been tested and used to implement the calculation scheme.

The first part of the study is dedicated to the validation of several lattice schemes for single assembly calculation with the purpose of maintaining consistency with the work currently performed both at IRSN and at EPM, and furthermore to highlight the sources of discrepancies that can be expected in the core calculation. The EPM has been working for several years to the implementation of up to date lattice schemes to be used on DRAGON5, focusing in particular on the development of an efficient two-level calculation scheme[6][7]. Hence, following the recent improvements in the geometry module of DRAGON5, different lattice schemes have been considered to generate the nuclear reactor database for full-core calculations. As example of new capability, it is now possible to define a windmill-type geometry discretization directly in the

code (through the `G2S:` module) without the need of external geometry CAD-software[8].

Following the single assembly calculation, the main aspect of the work has been to optimize the generation of the cross-sections database required to perform nodal core calculation according to GET theory. The validation tests were performed on a 3x3 cluster with different types of configuration(Figure 1). Following the recent work of Chambon[9], a methodology is studied for the different lattice schemes with the final aim of performing pin power reconstruction with the nodal solver PARCS.

The result both of lattice calculation and the core calculations are then validated using the stochastic code SERPENT2 [10]. The simulations have been performed with 1000 cycles of 1500000 source neutron each.

The purpose of the study has been to validate a calculation scheme between DRAGON5 and PARCS, through the modeling of a single assembly calculation to generate homogenized parameters; for this reason, the environmental effects have not been taken into account, and all the lattice calculation are performed in infinite lattice approximation.

| | | |
|---|---|---|
| UOX | UOX | UOX |
| UOX | FUEL | UOX |
| UOX | UOX | UOX |

Fig. 1. Representation of the 3x3-PWR colorset assembly configuration composed by a central fuel assembly (FUEL can be UOX, UOX with AIC control rods (UA) or MOX) and surrounded by UOX assemblies. Reflective boundary conditions are imposed.

## II. THEORY

In this section, a brief description of the homogenization theory is proposed[4][5]. The idea of homogenization is to replace the heterogeneous component with homogeneous one in order to reduce the computation time of large and complicated systems. The homogenized problem is also solved using a low order operator (derived as an asymptotic limit of the exact one) to eliminate some of the variables of the original problem.

Since it is not feasible to preserve all the details of the heterogeneous calculation, the purpose of the computation of a homogenized system is to obtain accurate global averaged values representative of the exact original system. Taking into account the loss of information, a choice has to be made to define the reference averaged values to be preserved by homogenization.

### 1. Equivalence Theory

A first step in the definition of a homogenized process is to choose reactors properties that should be reproduced by the homogeneous problem; only the preservation of the spatial integrals of quantities of interest is considered. Let's denote with "*" the solution of the exact heterogeneous problem and with "~" the correspondant homogeneous problem. For every energy group g and each cross-section, the following relations need to be satisfied:

- $\int_{V_i} \tilde{\Sigma}_g(\boldsymbol{r})\tilde{\phi}_g(\boldsymbol{r})d\boldsymbol{r} = \int_{V_i} \Sigma^*_g(\boldsymbol{r})\phi^*_g(\boldsymbol{r})d\boldsymbol{r}$
- $\int_{S^k_i} \boldsymbol{\nabla}\cdot\tilde{\boldsymbol{J}}_g(\boldsymbol{r})d\boldsymbol{S} = \int_{S^k_i} \boldsymbol{\nabla}\cdot\boldsymbol{J}^*_g(\boldsymbol{r})d\boldsymbol{S}$
- $k^*_{eff} = \tilde{k}_{eff}$

where $\phi_g(\boldsymbol{r})$ is the integrated flux, $\boldsymbol{J}_g(\boldsymbol{r})$ is the integrated current, $\Sigma_g$ is the total cross-section and $k_{eff}$ is the multiplication factor. So if the homogenized parameters are assumed to be spatially constant, for the region $i$ of volume $V_i$, an *ideal* homogenized cross-section can be defined by the first of the previous relations:

$$\tilde{\Sigma}^i_g = \frac{\int_{V_i} \Sigma^*_g(\boldsymbol{r})\phi^*_g(\boldsymbol{r})d\boldsymbol{r}}{\int_{V_i} \tilde{\phi}_g(\boldsymbol{r})d\boldsymbol{r}}. \tag{2}$$

The preservation of the integrated surface current instead depends on the low-order operator chosen to simplify the homogenized system. Since the nodal calculation will be solved in diffusion approximation only, this case will be presented. If the Fick law is assumed to define a heuristic relation between the neutron current and the gradient of the flux, it follows that:

$$\tilde{D}^i_g = \frac{-\int_{S^k_i} \boldsymbol{J}^*_g(\boldsymbol{r})d\boldsymbol{S}}{\int_{S^k_i} \boldsymbol{\nabla}\tilde{\phi}_g(\boldsymbol{r})d\boldsymbol{S}} \tag{3}$$

From the previous relation, it can be observed that nonlinearity is introduced since both the solution of the exact problem and the homogenized system must be known to satisfy Eqs. (2) and (3). Then an issue needs to be addressed to the definition of the homogenized diffusion coefficient of Eq. (3). Since each node is characterized by the $k$ surface, the same amount of diffusion coefficients need to be defined, and it is impossible to determine a unique spatially constant parameter that preserves both the average reaction rate and the surface-averaged group current.

To overcome the first problem, the most common employed practice is to obtain the exact solution by solving a 2-D heterogeneous transport equation on a limited part of the exact system (the assembly to be homogenized), assuming an infinite lattice calculation by imposing reflective boundary conditions. However, this method is particularly inaccurate when large spatial flux gradients are generated at the interface of different nodes, due to the use of spatially-constant diffusion

constants that are unable to solve the problem of preservation of surface integrate currents.

It can be observed that the continuity of flux at the interfaces is a limit for the diffusion calculation both to preserve reaction rates and surface current.

## 2. General Equivalence Theory

The General Equivalence Theory (GET) proposed by Smith [4], suggests the introduction of an additional degree of freedom to account for the preservation of the surface current. It provides discontinuity factors at each surface of the node in order to relax the continuity of fluxes and preserve both average reaction rates and net currents from the heterogeneous system. A new interface condition for each energy group is then defined to assure the continuity of the homogeneous flux between adjacent nodes:

$$f^{+}_{g,j} \int_{S_j} \tilde{\phi}^{+}_{g}(\boldsymbol{r}) d\boldsymbol{S} = f^{-}_{g,j} \int_{S_j} \tilde{\phi}^{-}_{g}(\boldsymbol{r}) d\boldsymbol{S} \tag{4}$$

Where $f^{+}_{g,j}$ and $f^{-}_{g,j}$ are the energy-dependent discontinuity factors at the surface $S_j$, $\tilde{\phi}^{+}_{g}$ and $\tilde{\phi}^{-}_{g}$ the surface average homogeneous fluxes, respectively. This relation assures the preservation of both reaction rates and net currents from heterogeneous reactor problems, by stating that the heterogeneous flux is continuous at the interface.

In the case where the heterogeneous solution is evaluated on a single assembly with reflective boundary conditions, the homogenized cross-sections and diffusion coefficient result to be equivalent to the flux-volume weighted one. Since the homogeneous flux can be assumed to be spatially flat in the homogenized node, and since the average heterogeneous flux and the averaged homogeneous flux are equal by definition, a new expression can be obtained:

$$\mathrm{adf}_{g,j} = \frac{\phi^{*}_{g,j}}{\bar{\phi}_{g,j}} \tag{5}$$

where $\mathrm{adf}_{g,j}$ is the assembly discontinuity factor (ADF) for each group and each surface of the node. This approach reduces the computational time and limits the calculation of equivalence parameters for each type of assembly.

## 3. Dehomogenization

Once the nodal calculation is performed, a reconstruction process is needed to regenerate the actual heterogenous structure inside each node. This procedure is usually called dehomogenization. The detailed description of the method implemented in PARCS is presented in the theory manual[11]. The output from the nodal flux solution is employed together with so called form functions to assure a proper reconstruction of the heterogenous power inside each node. Group Form Fuction (GFF) are computed from lattice calculation, considering the same approximation of ADF concerning the infinite lattice approximation. The GFF are groupwise factors defined as a function of the pincell fission rates as:

$$f_g(x,y) = \frac{\kappa\bar{\Sigma}_{fg}\varphi_g(x,y)}{\kappa\bar{\Sigma}_{fg}\bar{\varphi}_g} \tag{6}$$

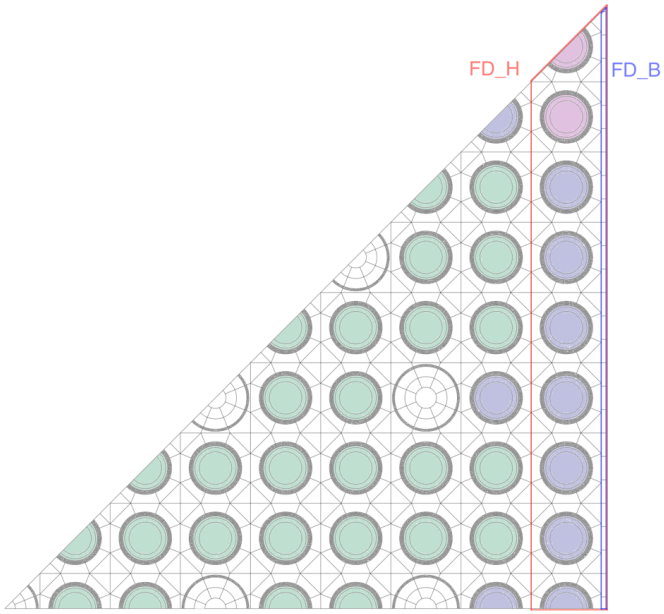


Fig. 2. Eight of PWR. In the picture are highlight the MOX distribution of enrichment, the windmill-type spatial discretization and the thin region where the surface flux is recovered in the thin region method

where $\kappa\bar{\Sigma}_{fg}$ is the macroscopic fission cross section of the fuel in group $g$ multiplied by the energy produced by fission. Due to the pin power reconstruction methodology, also so called Corner discontinuity factor (CDF), needs to be define to account for the local heterogeneities at the interface between assemblies. They are defined similarly to the ADFs, with the flux ricovered at the corner of the assembly:

$$\mathrm{cdf}_{g,j} = \frac{\phi^{*}_{g,j,corner}}{\bar{\phi}_{g,j}} \tag{7}$$

## III. MODELING

Different calculation schemes implemented in DRAGON5 have been tested on a representative motif. The geometry considered is a 3x3-PWR colorset assembly configuration with reflective boundary conditions comprising a center fuel assembly of AIC (UA) or MOX, surrounded by eight UOX assemblies (UOX) (Figure 1). The AIC assembly contains control rods made of a metal mixture composed of Silver, Indium, and Cadmium (AIC). The MOX assembly is designed with a three-zone Pu-content structure, where the content of Pu increase from the center towards the corner (Figure 2). In the diffusion calculation, nine assembly nodes are considered with the size corresponding to a lattice pitch in the radial plane, subsequently subdivided in 2x2 mesh each (4 nodes per assembly).

It should be noted that the colorset configuration has been chosen not to have a quasi-critical cluster and not to obtain a core critical configuration. The impact of leakage model of the lattice calculation is indeed of primary importance for

the evaluation of the result. Both the configurations with AIC and MOX assembly are chosen since a strong flux gradient is generated at the interface with the surrounding UOX assemblies, and it represents a challenge for nodal calculations with assembly homogenization. The impact of ADF indeed is supposed to be of primary importance.

The validation is carried out by comparing the diffusion calculation to a reference stochastic calculation performed with SERPENT2.

## 1. DRAGON5 Lattice Schemes

In this section, we give a brief description of the models that we implemented in the lattice calculation. Since the concepts behind the different schemes have been already deepened in other works[6][7][12][13][14], we proposed just a summary description of the principal characteristics that we implemented for the design of our lattice calculations.

Recently, Canbakan[7] developed a single level and two level schemes optimized for the SHEM295 refined energy mesh proposed by Hébert[15]. It has been designed to be employed with the Subgroup Projected Method (SPM) for the self-shielding calculation[15].

Regarding the two-level scheme, the main flux calculation is divided into two steps; after the resonance self-shielding calculation, a first-level double $P_1$ interface current calculation is performed over the 295-energy groups to collapse the cross section to 26-group. A detailed second level flux calculation is then performed using the method of characteristics (MOC) on the 26-group mesh. Following the developments in the `G2S:` module of DRAGON5[8], it is now possible to generate a windmill-type spatial discretization (Figure 2) for the detailed MOC calculation without the use of an external software.

The single level scheme is performed instead without an intermediate condensation to a coarser energy mesh, and the MOC fine calculation is conducted using the 295 energy groups self-shielded library. It should be remarked that an SPH equivalence technique can be implemented in the 2 level scheme between the 26 group condensation and the fine flux calculation; we decided to run our simulation with both the possibilities.

A different two level scheme precedently employed at EPM was the one described in the study of Vallerent[6]. Since the first part of the project has been made with this methodology, we decided to maintain it, only substituting the old inefficient spatial mesh with the new windmill-type discretization. It is characterized by the use of the SHEM 281 energy mesh, and the self-shielding calculation is performed with the statistical subgroup method with physical probability tables (ST method) implemented in DRAGON5[16]. The same 2 level approach is employed as in Cabakan, and according to the analysis of Vallerent, an SPH equivalence is performed between the two levels. Both the 2 level calculation scheme are based on the REL2005 logic developed by CEA[12].

Regarding the ORION project, the so-called DRAGOR-V1 calculation scheme is produced with DRAGON5 using a single level approach based on the CEA-97 scheme developed by CEA[13]. A 172 group energy mesh is considered both for the flux and the self-shielding calculation, performed with a similar methodology as in the Vallerent scheme. The spatial mesh is characterized by a simple discretization, without any subdivision of the moderator in the pin cell.

The cross-section libraries used for the calculations are DRAGLIB format libraries, based on the evaluation JEFF 3.1.1. Only for the CEA-97 based scheme of IRSN, we decided to use the original JEF 2.2 library. A similar comparison has already been made[1], and we expect the appearance of discrepancies due to the different nuclear data evaluation.

To summarize, five different DRAGON5 runs have been performed to maintain consistency with the work currently performed both for the ORION project and at École Polytechnique de Montréal:

1. *Canb 2lvl SPH*
   (a) SHEM295
   (b) SPM self-shielding
   (c) 2 level scheme (IC 295gr + MOC 26gr)
   (d) SPH equivalence at 26gr
   (e) windmill-type mesh
2. *Canb 2lvl w/o SPH*
3. *Canb 1lvl*
   (a) SHEM295
   (b) SPM self-shielding
   (c) 1 level scheme (MOC 295gr)
   (d) windmill-type mesh
4. *Vall WM 2lvl*
   (a) SHEM281
   (b) ST self-shielding
   (c) 2 level scheme (IC 295gr + MOC 26gr)
   (d) SPH equivalence at 26gr
   (e) windmill-type mesh
5. *DRAGOR-V1 1lvl*
   (a) JEF 2.2 172gr
   (b) ST self-shielding
   (c) 1 level scheme (IC 172gr)
   (d) simple mesh

Three options are evaluated concerning the flux calculation and the leakage model: without any leakage model, with a $B_1$ homogeneous leakage, and with a $P_1$ homogeneous leakage[16][17]. In the first case, the eigenvalue to be computed is the effective multiplication factor with a fixed buckling equal to zero. For the other two cases, the eigenvalue is the critical buckling, and the effective multiplication factor is imposed equal to unity (consider a critical assembly). It should be remarked that a nasty situation happens with the $B_1$ model in some low-reactivity cases[16]. For this reason, in the newest version of DRAGON5, a dynamic correction is

performed such that the $B_1$ model is replaced by the $P_1$ model if particular subcritical conditions occur. However, this is not the case for our study.

At the end of the calculation, the flux is used to collapse cross-sections to two groups (threshold at 0.625 eV), and the homogenization is performed over the whole assembly. The generated nuclear data are then stored in a DRAGON5 data structure of type `MULTICOMPO`; it also contains the information required to compute ADF, CDF, and GFF.

It should be noted that the geometry considered is an eight of assembly, specified for the North-East quadrant(Figure 2). The gas gap has not been explicitly designed but diluted in the metal mixture for the cladding; furthermore, the grid has been diluted in the moderator generating five different compositions related to the position inside the fuel assembly.

### 2. Computation of ADF,CDF and GFF

Different evaluations can be done to generate the surface flux required to compute the ADFs. Indeed, using the `EDI` module of DRAGON, usually two methods are used to recover the surface flux[8]:

- direct interface current (IC) method;
- thin regions method.

In the direct IC method, the surface flux is obtained by direct homogenization of the interface currents of the pins corresponding to the outer row. Once the outgoing current is computed, the following relation is employed to calculate the surface flux:

$$\phi_{surf} = \frac{4J_{out}}{S} \tag{8}$$

where $\phi_{surf}$ is the boundary flux, $J_{out}$ is the outgoing interface current and $S$ the correspondant surface. This method is available only when the IC method is used to perform the flux calculation.

The thin regions method instead consists of defining a thin outer region close to the external surface of the assembly and assuming that the volumic flux in this small region is equivalent to a corresponding surface flux. In this work, two options of the volume have been studied for the computation of the surface flux (Figure 2):

- The water gap (case `FD_B`);
- The outer pin row facing the side of the assembly and its surrounding water gap (case `FD_H`).

For all the lattice schemes where the MOC flux calculation is performed considering the windmill-type geometry, only the thin region method has been contemplated. However, in the single level *DRAGOR-V1 1lvl* scheme is not possible to apply the same methodology because the water gap region is not explicitly discretized. Instead, the direct IC method has been adopted, and we are going to refer to it as *FD_B* for the *DRAGOR-V1 1lvl* case. The modification has been performed directly during the lattice calculation taking advantage of the utility modules of DRAGON5.

The CDF are defined similarly to the ADF, applying the thin regions method in the corner region of the assembly. Specifically, we decided to recover the corner flux on the square area at the top of the water gap when the windmill discretization has been implemented. In the case of *DRAGOR-V1 1lvl* scheme, for the same reasons highlight for the ADFs, we recover the corner flux in the corner pin.

Regarding the computation of the GFFs, since an automated procedure is not yet implemented for the windmill-type geometry in homogenization module of DRAGON5, the number of regions to be homogenized need to be defined explicitly. As already observed by Chambon, it should be highlight that the Group form factors should be computed in the outer pin row without including the water gap. For the *DRAGOR-V1 1lvl* case, since the water gap is included in the last row of pins, a volume correction is performed following the pin power reconstruction. Each value in the power map is multiplied for the correspondent ratio between the homogenization volume and the reference volume of the pin cell (fuel,cladding and moderator); in the case of the *DRAGOR-V1 1lvl* scheme, the homogenization volume contains the water gap and the ratio is greater then one.

### 3. Cross-Section Preparation

The macroscopic cross-section data generated by the lattice calculation with DRAGON5 are stored in a `MULTICOMPO` data structure to be reprocessed and to generate an input file for the nodal code PARCS. The GenPMAXS utility[18] is not able to read a `MULTICOMPO` data structure as produced by DRAGON5. A procedure has been developed to transform the `MULTICOMPO` object into an HELIOS-like data file, before calling the GenPMAXS utility. The `NCR:` and `D2P:` modules of DONJON5 allow to interpolate the values of the `MULTICOMPO`, compute the ADF and reformats the reactor database into an input file readable by the GENPMAXS utility which in turn will create a PMAX file, the input file for PARCS simulation.

## IV. RESULTS AND ANALYSIS

The discussion of the results will be presented in this chapter, separately for the lattice and the diffusion calculation.

### 1. Lattice calculation

To investigate the accuracy of the lattice calculation we consider the Canbakan validation[7]; the comparison is performed with no leakage approximation. For each type of fuel assembly, and for each lattice scheme, we first compare the effective multiplication factor and the reactivity evaluated as:

$$\Delta\rho = \left(\frac{1}{k_{eff}(S2)} - \frac{1}{k_{eff}(D5)}\right) \cdot 10^5 \tag{9}$$

where $k_{eff}(S2)$ and $k_{eff}(D5)$ are the effective multiplication factors of SERPENT2 and DRAGON5. The results are presented in Table I. An overall agreement can be observed for the *Canb 2lvl SPH* and *Vall WM 2lvl* schemes, with a wider difference only in the MOX case. For the former, the SPH equivalence generates a significant degrading for all the configuration. Furthermore, the *Canb 1lvl* scheme exhibits only a significative discrepancy for the rodded case, while for the

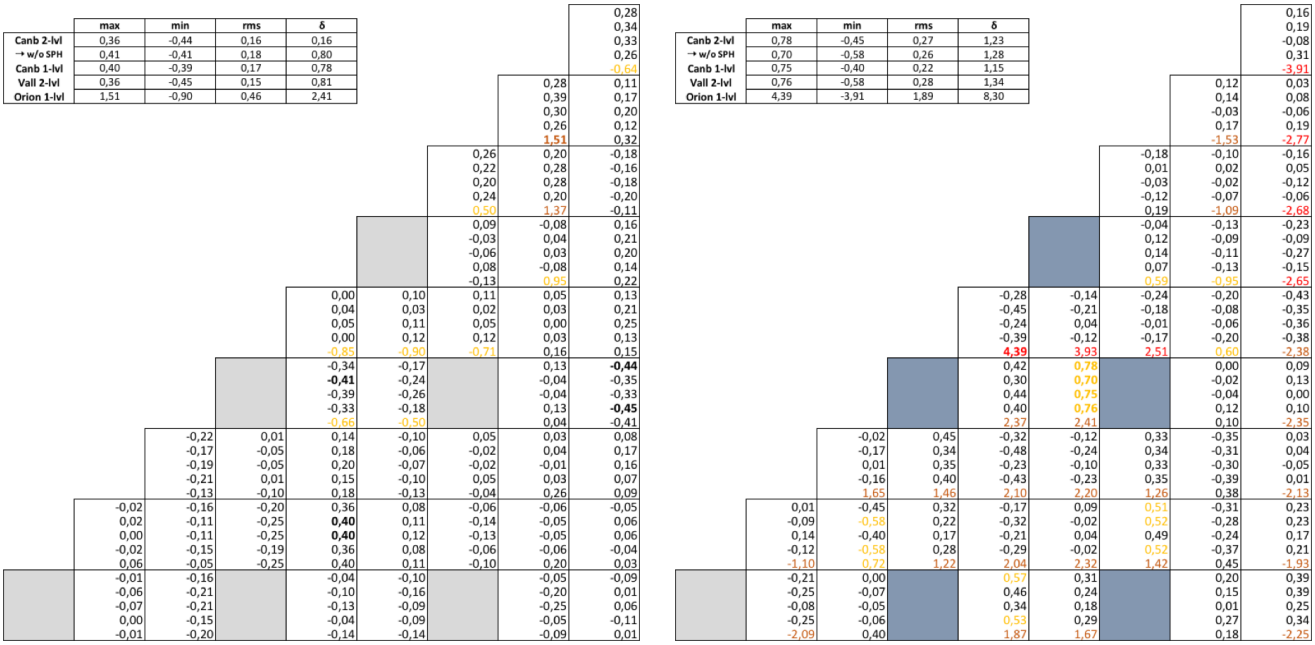

| | max | min | rms | δ |
|---|---|---|---|---|
| Canb 2-lvl | 0,36 | -0,44 | 0,16 | 0,16 |
| → w/o SPH | 0,41 | -0,41 | 0,18 | 0,80 |
| Canb 1-lvl | 0,40 | -0,39 | 0,17 | 0,78 |
| Vall 2-lvl | 0,36 | -0,45 | 0,15 | 0,81 |
| Orion 1-lvl | 1,51 | -0,90 | 0,46 | 2,41 |

| | max | min | rms | δ |
|---|---|---|---|---|
| Canb 2-lvl | 0,78 | -0,45 | 0,27 | 1,23 |
| → w/o SPH | 0,70 | -0,58 | 0,26 | 1,28 |
| Canb 1-lvl | 0,75 | -0,40 | 0,22 | 1,15 |
| Vall 2-lvl | 0,76 | -0,58 | 0,28 | 1,34 |
| Orion 1-lvl | 4,39 | -3,91 | 1,89 | 8,30 |

Fig. 3. Relative discrepancies in the fission reaction map for the UOX (left) and the UA (right) assembly

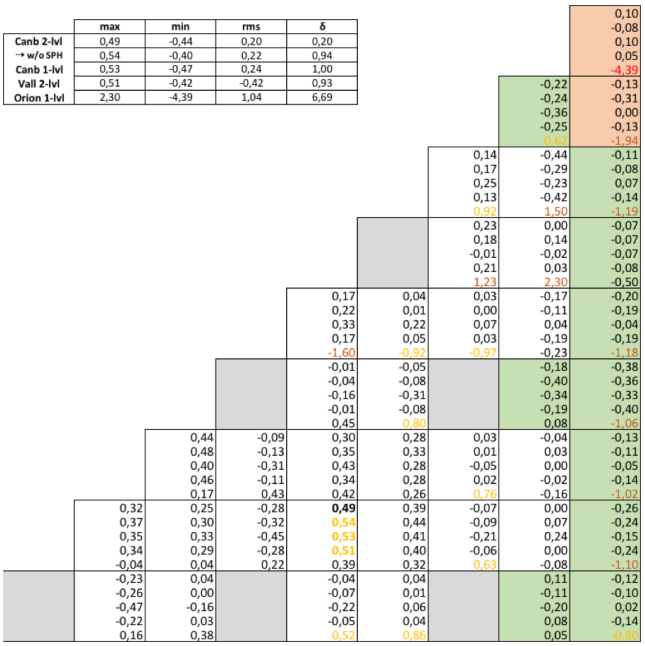

| | max | min | rms | δ |
|---|---|---|---|---|
| Canb 2-lvl | 0,49 | -0,44 | 0,20 | 0,20 |
| → w/o SPH | 0,54 | -0,40 | 0,22 | 0,94 |
| Canb 1-lvl | 0,53 | -0,47 | 0,24 | 1,00 |
| Vall 2-lvl | 0,51 | -0,42 | -0,42 | 0,93 |
| Orion 1-lvl | 2,30 | -4,39 | 1,04 | 6,69 |

Fig. 4. Relative discrepancies in the fission reaction map in the MOX assembly

| | UOX | | UA | | MOX | |
|---|---|---|---|---|---|---|
| | $k_\infty$ | $\Delta\rho_{tr}$ | $k_\infty$ | $\Delta\rho_{tr}$ | $k_\infty$ | $\Delta\rho_{tr}$ |
| SERPENT2 | 1.382080 | | 0,924720 | | 1,163170 | |
| *Canb 2lvl SPH* | 1.381282 | -42 | 0.926385 | 194 | 1.161150 | -150 |
| *Canb 2lvl w/o SPH* | 1.379066 | -158 | 0.921427 | -386 | 1.159602 | -265 |
| *Canb 1lvl* | 1.382942 | 45 | 0.928084 | 392 | 1.164670 | 111 |
| *Vall WM 2lvl* | 1.380812 | -66 | 0.926436 | 200 | 1.160184 | -221 |
| *DRAGOR-V1 1lvl* | 1.385929 | 201 | 0.920391 | -509 | 1.160870 | -170 |

TABLE I. $k_{eff}$ and reactivitiy [$pcm$] for the different fuel assembly. Without leakage model.

| | | UOX | | | | UA | | | |
|---|---|---|---|---|---|---|---|---|---|
| | | U235 | | U238 | | U235 | | U238 | |
| | *group* | $\Delta r$ | $\Delta a$ | $\Delta r$ | $\Delta a$ | $\Delta r$ | $\Delta a$ | $\Delta r$ | $\Delta a$ |
| *Canb 2lvl SPH* | 1 | 0.1 | 14.6 | -0.3 | -68.0 | -0.2 | -25.8 | -0.7 | -155.2 |
| | 2 | 0.1 | 58.3 | 0.1 | 3.5 | -1.6 | 96.6 | -0.7 | 8.6 |
| | tot | | 72.9 | | -64.5 | | 70.8 | | -146.6 |
| *Canb 2lvl w/o SPH* | 1 | 0.9 | 108.2 | 0.4 | 88.1 | 0.7 | 85.6 | 0.3 | 58.0 |
| | 2 | -0.0 | -13.8 | -0.1 | -4.7 | -1.6 | 96.6 | -0.7 | 8.6 |
| | tot | | 94.4 | | 83.3 | | 83.1 | | 55.5 |
| *Canb 1lvl* | 1 | -0.2 | -27.2 | -0.7 | -155.0 | -0.7 | -81.4 | -1.2 | -270.1 |
| | 2 | 0.1 | 64.2 | 0.1 | 3.9 | 0.4 | 113.0 | 0.3 | 10.2 |
| | tot | | 37.0 | | -151.2 | | 31.6 | | -259.9 |
| *Vall WM 2lvl* | 1 | 0.1 | 9.6 | 0.0 | 9.2 | -0.3 | -29.5 | -0.3 | -77.8 |
| | 2 | 0.1 | 55.4 | 0.1 | 3.2 | 0.3 | 92.9 | 0.2 | 8.3 |
| | tot | | 65.0 | | 12.4 | | 63.4 | | -69.5 |
| *DRAGOR-V1 1lvl* | 1 | -1.0 | -113.0 | 0.5 | 116.5 | -0.8 | -92.7 | 0.8 | 192.8 |
| | 2 | -0.5 | -280.9 | 0.2 | 13.1 | -0.9 | -292,48 | -0.2 | -5.8 |
| | tot | | -393.9 | | 129.6 | | -385.2 | | 187.0 |

TABLE II. Absorption Rate accuracy for UOX and UA assembly. Without leakage model.

| | | MOX | | | | | | | | | |
|---|---|---|---|---|---|---|---|---|---|---|---|
| | | U235 | | U238 | | Pu239 | | Pu240 | | Pu241 | |
| | *group* | $\Delta r$ | $\Delta a$ | $\Delta r$ | $\Delta a$ | $\Delta r$ | $\Delta a$ | $\Delta r$ | $\Delta a$ | $\Delta r$ | $\Delta a$ |
| *Canb 2lvl SPH* | 1 | 0.09 | 0.53 | -0.13 | -27.74 | -0.31 | -1.04 | 0.51 | 67.26 | 0.29 | 35.23 |
| | 2 | 0.77 | 3.54 | 0.61 | 5.58 | 1.11 | 3.40 | -0.09 | -29.50 | 0.25 | 7.74 |
| | tot | | 4.07 | | -22.17 | | 2.36 | | 37.76 | | 42.98 |
| *Canb 2lvl w/o SPH* | 1 | 0.94 | 5.47 | 0.47 | 99.17 | 0.30 | 1.01 | 1.35 | 178.09 | 0.41 | 50.20 |
| | 2 | 0.31 | 1.41 | 0.17 | 1.58 | 0.61 | 1.85 | -0.46 | -153.75 | -0.07 | -2.04 |
| | tot | | 6.88 | | 100.75 | | 2.86 | | 24.35 | | 48.16 |
| *Canb 1lvl* | 1 | -0.63 | -3.62 | -0.79 | -164.06 | -0.81 | -2.70 | -0.09 | -11.75 | -0.72 | -88.58 |
| | 2 | 1.24 | 5.79 | 1.03 | 9.54 | 1.68 | 5.18 | 0.06 | 20.69 | 0.46 | 14.34 |
| | tot | | 2.17 | | -154.52 | | 2.48 | | 8.94 | | -74.24 |
| *Vall WM 2lvl* | 1 | -0.48 | -2.76 | 0.34 | 71.33 | -0.06 | -0.20 | 1.82 | 240.76 | 0.59 | 72.75 |
| | 2 | 0.40 | 1.85 | 0.24 | 2.20 | 0.75 | 2.27 | -0.47 | -157.30 | -0.13 | -4.05 |
| | tot | | -0.92 | | 73.53 | | 2.08 | | 83.45 | | 68.71 |
| *DRAGOR-V1 1lvl* | 1 | -2.30 | -13.02 | 0.89 | 188.40 | -7.90 | -24.58 | 0.20 | 25.89 | 1.82 | 227.53 |
| | 2 | 0.21 | 0.97 | 0.90 | 8.27 | 1.61 | 4.93 | -0.90 | -302.38 | 0.91 | 28.52 |
| | tot | | -12.05 | | 196.67 | | -19.65 | | -276.49 | | 256.05 |

TABLE III. Absorption Rate accuracy for MOX. Without leakage model.

*DRAGOR-V1 1lvl* scheme, we observe the highest difference in reactivity (more than 500 pcm).

The second parameter that had been analyzed is the total isotopic absorption rate inside the fuel. Only $U235$ and $U238$ are presented for the UOX and UA, while the three principal isotopes of *Pu* are also displayed for the MOX fuel. To conduct the comparison, the total absorption rate of the SERPENT2 calculation has been normalized on the total fission rate of DRAGON5, so that the relative and absolute differences are evaluated as:

$$\Delta r = \left(\frac{\tau_{D5} - \tau_{S2}}{\tau_{S2}}\right) \cdot 100 \tag{10}$$

$$\Delta a = (\tau_{D5} - \tau_{S2}) \cdot 10^5 \tag{11}$$

where $\tau_{D5}$ and $\tau_{S2}$ are the integrated absorption rate obtained with DRAGON5 and SERPENT2. The *DRAGOR-V1 1lvl* scheme presents the worst results for all the cases, with the highest absolute difference that is slightly below 400 pcm for the UOX case. Different trends can be seen for the others lattice schemes, depending on the fuel. In the case of fuel

| | UA-UOX | | | | | | MOX-UOX | | | | | |
|---|---|---|---|---|---|---|---|---|---|---|---|---|
| | FD_B | | FD_H | | NO ADF | | FD_B | | FD_H | | NO ADF | |
| | $k_{eff}$ | $\Delta\rho$ | $k_{eff}$ | $\Delta\rho$ | $k_{eff}$ | $\Delta\rho$ | $k_{eff}$ | $\Delta\rho$ | $k_{eff}$ | $\Delta\rho$ | $k_{eff}$ | $\Delta\rho$ |
| *Canb 2lvl SPH* | 1.33621 | -348 | 1.33594 | -363 | 1.33350 | -500 | 1.35296 | -248 | 1.35269 | -262 | 1.35266 | -264 |
| *Canb 2lvl w/o SPH* | 1.33381 | -482 | 1.33354 | -498 | 1.33108 | -637 | 1.35081 | -366 | 1.35054 | -380 | 1.35051 | -382 |
| *Canb 1lvl* | 1.33794 | -251 | 1.33766 | -267 | 1.33519 | -405 | 1.35491 | -141 | 1.35463 | -157 | 1.35461 | -158 |
| *Vall WM 2lvl* | 1.33600 | -360 | 1.33572 | -375 | 1.33324 | -515 | 1.35259 | -268 | 1.35232 | -283 | 1.35230 | -284 |
| *DRAGOR-V1 1lvl* | 1.33959 | -159 | 1.33959 | -159 | 1.33746 | -278 | 1.35736 | -8 | 1.35717 | -19 | 1.35717 | -18 |

TABLE IV. $k_{eff}$ and reactivitiy [$pcm$] for the motif UA-UOX (Reference SERPENT2 $k_{eff} = 1.34245$) and MOX-UOX (Reference SERPENT2: $k_{eff} = 1.35751$). $B_1$ homogeneous leakage model.

| | UA-UOX | | | | | | | | | MOX-UOX | | | | | | | | |
|---|---|---|---|---|---|---|---|---|---|---|---|---|---|---|---|---|---|---|
| | FD_B | | | FD_H | | | NO ADF | | | FD_B | | | FD_H | | | NO ADF | | |
| | Crn | Ctr | Side | Crn | Ctr | Side | Crn | Ctr | Side | Crn | Ctr | Side | Crn | Ctr | Side | Crn | Ctr | Side |
| *Canb 2lvl SPH* | -0.26 | 2.53 | -0.07 | -0.27 | 3.32 | -0.18 | -0.27 | 10.81 | -1.23 | -0.76 | 4.46 | -0.08 | -0.79 | 6.66 | -0.50 | -0.76 | 7.78 | -0.76 |
| *Canb 2lvl w/o SPH* | -0.21 | 2.07 | -0.07 | -0.21 | 2.87 | -0.18 | -0.21 | 10.41 | -1.23 | -0.77 | 4.49 | -0.09 | -0.80 | 6.71 | -0.50 | -0.76 | 7.82 | -0.76 |
| *Canb 1lvl* | -0.29 | 2.68 | -0.06 | -0.30 | 3.51 | -0.17 | -0.31 | 11.06 | -1.23 | -0.82 | 4.74 | -0.08 | -0.86 | 7.02 | -0.50 | -0.82 | 8.13 | -0.76 |
| *Vall WM 2lvl* | -0.26 | 2.42 | -0.06 | -0.27 | 3.25 | -0.17 | -0.27 | 10.83 | -1.23 | -0.76 | 4.49 | -0.10 | -0.79 | 6.70 | -0.51 | -0.76 | 7.77 | -0.76 |
| *DRAGOR-V1 1lvl* | -0.16 | 3.09 | -0.26 | -0.15 | 3.14 | -0.28 | -0.14 | 9.50 | -1.19 | -0.72 | 5.25 | -0.28 | -0.76 | 6.57 | -0.51 | -0.73 | 7.41 | -0.72 |

TABLE V. Assembly Power (% difference) for the motif UA-UOX and MOX-UOX. $B_1$ homogeneous leakage model. Crn=corner assembly, Ctr=Center Assembly and Side=Side Assembly

UOX, largest errors are observed for the $U238$ respect the $U235$. In this cases, the SPH equivalence seems to generate a degradation of the absorption. The best trending is observed for the *Vall WM 2lvl* scheme.

For the fuel MOX, high compensations between the two energy groups are observed for the $Pu240$. In the *Canb 2lvl SPH* scheme, the results are quite improved respect the precedent cases.

Finally, the fission reactions map is presented for the three cases. It is interesting because it allows a primary evaluation of the GFFs, required for the pin power reconstruction. All the cases except the *DRAGOR-V1 1lvl* scheme present the same general tendencies. The maximum value oscillates from 0.40% for the UOX case to a peak of 0.78% for the UA one. A similar trend can be observed for all the schemes. The *DRAGOR-V1 1lvl* scheme, however, presents vast discrepancies with a maximum absolute peak of 4.39% both for the UA and the MOX case. For all the options, the root means square errors are well beyond the other schemes. It should be observed that the highest differences are located in the outer pin row, and they may be related to the pin discretization and the homogenization procedure.

## 2. Core calculation

The reactor database generated with the lattice calculation is assessed for two configurations of the colorset 3x3: with AIC assembly (UA-UOX) and with MOX assembly (MOX-UOX) at the center of the motif. For all the lattice schemes, three option will be displayed (`FD_B`,`FD_H`,`NO ADF`) to highlight the impact of the methodologies implied for the computation of the ADFs. It should be recalled that the ADF option `NO ADF` corresponds to a diffusion calculation with PARCS run with ADF equal to unity. Only the $B_1$ homogeneous model as leakage approximation for the lattice calculation is presented in this study. Few remarks are later made to justify this choice.

The PARCS runs were performed with the default solver (HYBRID).

The results from the diffusion computation are assessed through the comparison between the reactivity, the assembly power maps, and the pin power map generated by PARCS and the values computed with the stochastic calculation with SERPENT2. The reactivity is evaluated in the same fashion as in Eq. (9). Regarding the assembly power and the pin powers, the results of SERPENT2 are normalized respect the total power computed from the PARCS estimate. For the assembly power, we considered only three representative assemblies (Corner, Center, and Side), taking advantage of the symmetry of the problem.

We first investigate the reactivity and the assembly power presented in Table VIII and IX.

Despite what has been assessed during the lattice evaluation, among the several schemes implemented, the *DRAGOR-V1 1lvl* option seems the best alternative for what concern the reactivity, however with a degraded outcome for the assembly power. An overall general agreement can be observed for all the other cases, with discrepancies in reactivity enclosed around 200 pcm and with errors of power limited to few tenths of percentage for some assembly of the cluster. The *Canb 2lvl SPH* scheme seems overall the best alternative, as a trade-off between the different results. The implementation of ADFs gives an improvement in all the schemes under analysis, with an overall gain in accuracy. The `FD_B` option seems to represent the best alternatives with a slight improvement if compared to the `FD_H` case.

The results from the pin power reconstruction are then presented in the figures 5 and 6, and summarized in tables VI and VII for both configurations.

The pin power map does not agree rigorously with what has been assessed in the previous analysis. The primary consideration is that the overall best results are achieved with the `FD_H` option for the UA cluster and with the `FD_B` option

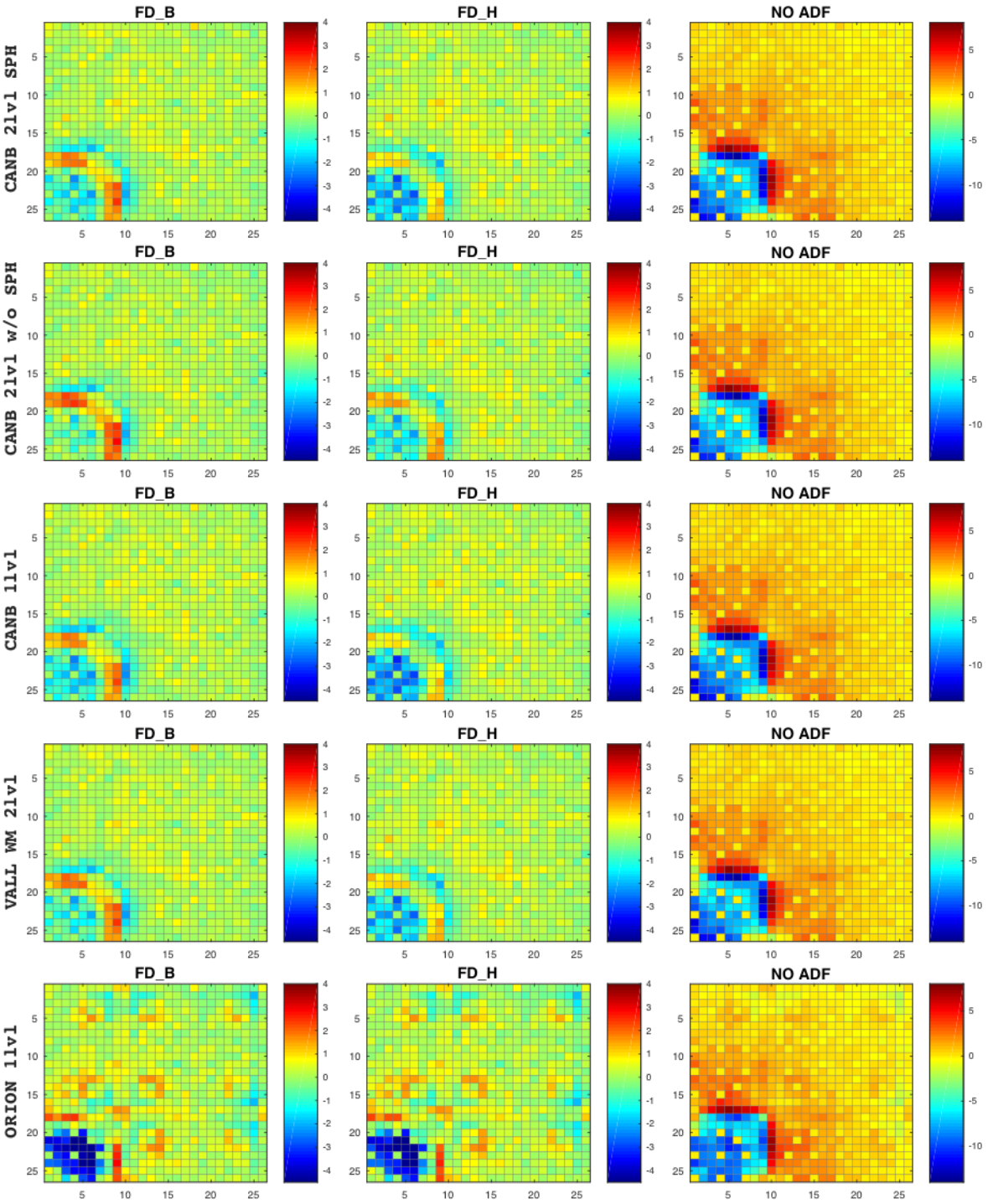


Fig. 5. Pin power error maps for the UA-UOX case (Quarter representation). All the lattice schemes are displayed together with all the options considered for the ADFs.

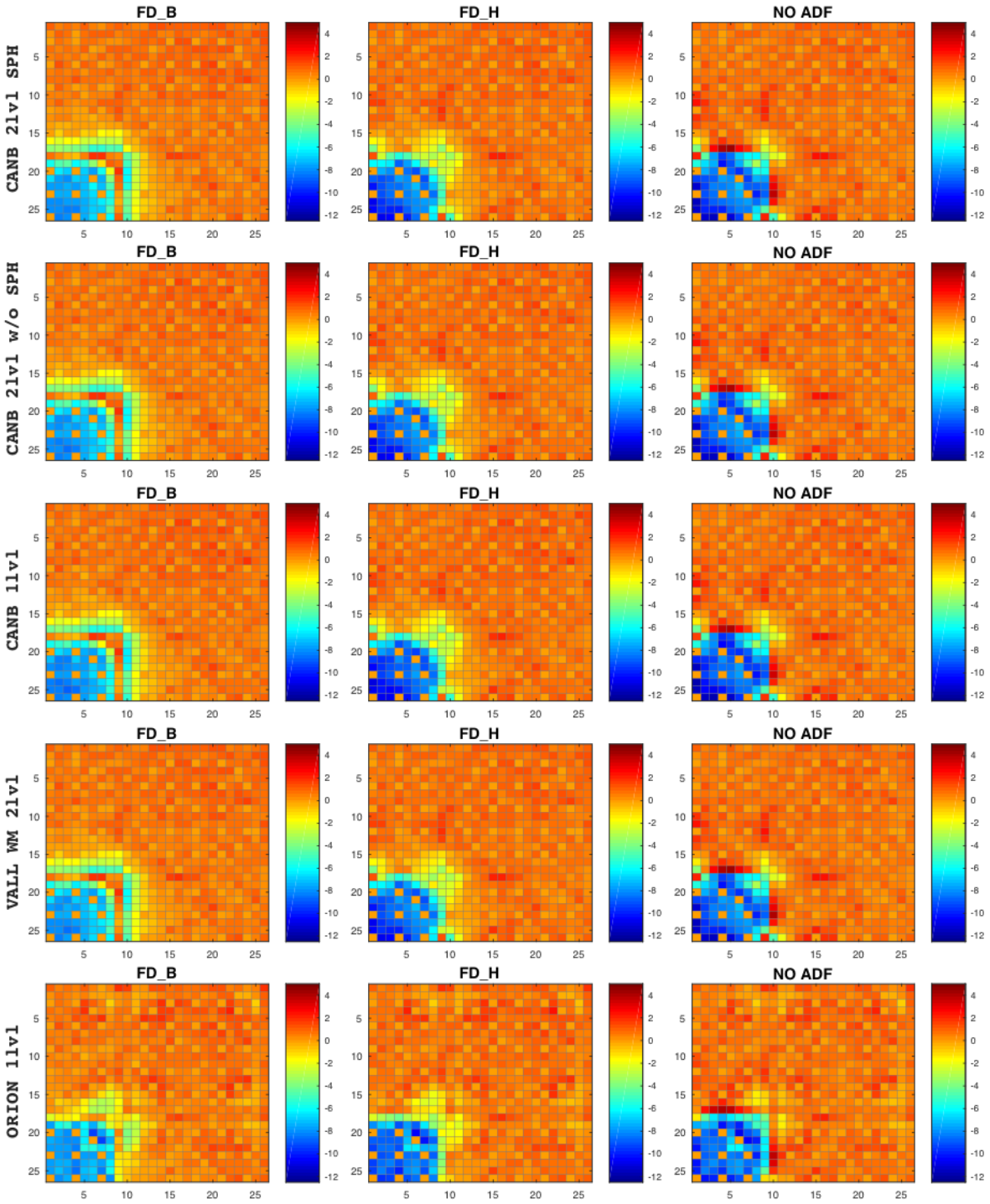


Fig. 6. Pin power error maps for the MOX-UOX case (Quarter representation). All the lattice schemes are displayed together with all the option considered for the ADFs.

| | FD_B | | | | FD_H | | | | NO ADF | | | |
|---|---|---|---|---|---|---|---|---|---|---|---|---|
| | max | min | rms | $\delta$ | max | min | rms | $\delta$ | max | min | rms | $\delta$ |
| *Canb 2lvl SPH* | 2.68 | -2.72 | 0.57 | 5.40 | 1.71 | -3.33 | 0.59 | 5.04 | 7.39 | -13.58 | 2.88 | 20.97 |
| *Canb 2lvl w/o SPH* | 3.05 | -2.68 | 0.57 | 5.74 | 2.11 | -2.74 | 0.53 | 4.85 | 7.49 | -13.40 | 2.77 | 20.89 |
| *Canb 1lvl* | 2.67 | -2.94 | 0.59 | 5.61 | 1.59 | -3.56 | 0.63 | 5.16 | 7.12 | -13.68 | 2.94 | 20.81 |
| *Vall WM 2lvl* | 2.76 | -2.72 | 0.57 | 5.47 | 1.80 | -3.27 | 0.57 | 5.07 | 7.34 | -13.63 | 2.88 | 20.97 |
| *DRAGOR-V1 1lvl* | 3.38 | -6.99 | 1.03 | 10.37 | 3.13 | -6.93 | 1.02 | 10.06 | 7.60 | -11.33 | 2.80 | 18.94 |

TABLE VI. Pin Power (% difference) for the colorset UA-UOX. $B_1$ homogeneous leakage model.

| | FD_B | | | | FD_H | | | | NO ADF | | | |
|---|---|---|---|---|---|---|---|---|---|---|---|---|
| | max | min | rms | $\delta$ | max | min | rms | $\delta$ | max | min | rms | $\delta$ |
| *Canb 2lvl SPH* | 2.32 | -9.14 | 2.18 | 11.46 | 2.58 | -11.03 | 2.49 | 13.61 | 4.23 | -12.04 | 2.75 | 16.27 |
| *Canb 2lvl w/o SPH* | 2.28 | -9.23 | 2.19 | 11.51 | 2.49 | -11.03 | 2.51 | 13.52 | 4.18 | -12.06 | 2.77 | 16.23 |
| *Canb 1lvl* | 2.12 | -9.58 | 2.28 | 11.70 | 2.52 | -11.30 | 2.62 | 13.82 | 3.92 | -12.30 | 2.87 | 16.22 |
| *Vall WM 2lvl* | 2.28 | -9.16 | 2.17 | 11.44 | 2.60 | -11.02 | 2.50 | 13.61 | 4.28 | -11.98 | 2.75 | 16.26 |
| *DRAGOR-V1 1lvl* | 2.51 | -9.55 | 2.22 | 12.06 | 2.54 | -10.56 | 2.51 | 13.10 | 4.17 | -11.04 | 2.69 | 15.21 |

TABLE VII. Pin Power (% difference) for the colorset MOX-UOX. $B_1$ homogeneous leakage model.

for the MOX one. The highest errors are localized mostly at the interfaces and in the inner zone of the interior assembly, depending on the configuration. The range of errors does not deviate significantly between the lattice schemes, with the *Vall WM 2lvl* option presenting the best overall results.

Only the *DRAGOR-V1 1lvl* scheme displays a peculiar behavior for the UA-UOX configuration. It can be remarked from the error power map that large errors are concentrated in the region surrounding the absorber rods, particularly when the ADFs are implemented. Besides, the root means square errors exhibit a greater extent respect the other alternatives. Bearing in mind the results from the lattice validation, the homogenized cross-sections and GFFs may be addressed as a possible source of inaccuracies, since the ADFs can be correlated to a predominant local effect.

The magnitude of the discrepancies agrees with what has been assessed by Chambon[9].

### *A. Leakage Model*

We decided to present only the results from the $B_1$ homogeneous leakage approximation. The reason to exclude an approach without leakage derives from the fact that we privileged a realistic configuration adaptable for an industrial application. However, it should be remarked that the absence of a leakage model may originate better results for some simulations. In particular, we observed that the best results for the MOX-UOX configuration (*rms* between 1.10% and 1.70%) had been reached considering lattice calculations performed without any leakage model and with the FD_B option for ADF. This phenomenon should be reconducted to the infinite lattice approximation employed in the assembly calculation and the particular case of study chosen for the validation.

For what concern the $P_1$ homogeneous model, the results are shown in the Appendix. We first observed that if we consider the reactivity and the assembly power errors, the $P_1$ method produces worst result compared to the $B_1$ approximations. Furthermore, besides limited combinations of calculation options, the same assessment can be done for the pin power discrepancies, with the reconstructed values slightly degraded respect the $B_1$ leakage model. Even if a recent work strongly supports the use of $P_1$ rather than the $B_1$ method[19], for our particular configuration and the methods that we implemented to generate the homogenized parameters, our calculations show a better solution coming from the $B_1$ method. Since we hypothesize that the $B_1$ method should be preferred to the $P_1$, we decided to present only the former method.

### *B. ADF*

For all the methods of validation, the implementation of ADFs provides a clear improvement for all calculation schemes under analysis. If we consider only the reactivity and the assembly powers, for all the computations, the FD_B option should be preferred respect the FD_H one (surface flux recovered in the smaller outer region). Furthermore, the results from the pin power map show that the value of the ADFs strongly affects the reconstruction process, leading to an overall improvement of the pin power values. However, the entity of these ameliorations vary according to the problem.

To highlight the impact of the ADFs, a detailed examination is conducted through the explicit representations of the pin power map for the UA-UOX and MOX-UOX configurations obtained for the *Canb 2lvl SPH* scheme with ADF options FD_B and NO ADF. They are presented in figures 7 and 8 respectively.

For the configuration containing the rodded assembly, the employment of the ADFs profoundly reduces the error in the central part of the motif, leaving only marked differences at the interface between the UA and UOX assemblies. For the MOX-UOX case instead, this impact is less pronounced, and it consists mostly in a slight reduction of the discrepancies in the region of the motif surrounding the central assembly. Following the observations made concerning the leakage model, we hypothesize that if the environment is taken into account correctly, a higher effectiveness of ADF should be exhibited.

### *C. GFF and CDF*

In the present study, we are not presenting the case where both GFF and CDF are set equal to unity, and any calculation

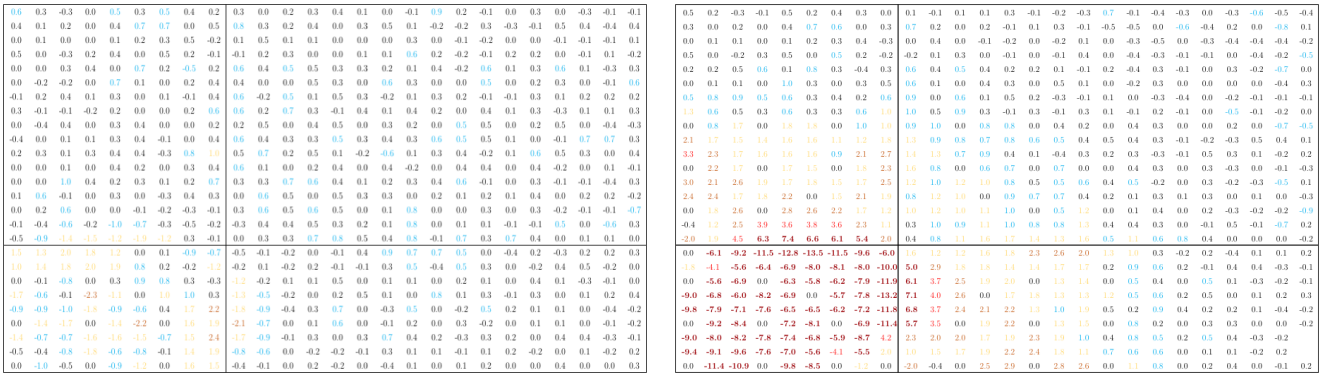

Fig. 7. Relative discrepancies in the pin power map in the UA-UOX configuration. $B_1$ homogeneous model. `FD_B` (left) and `NO ADF` (right) option. Canbakan 2 level scheme with SPH equivalence.

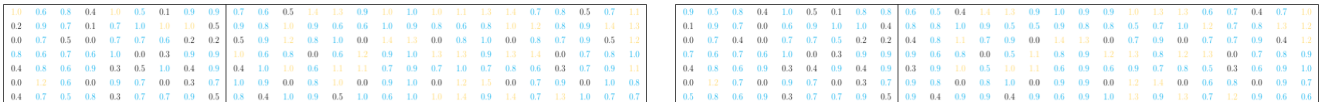

Fig. 8. Relative discrepancies in the pin power map in the MOX-UOX configuration. $B_1$ homogeneous model. `FD_B` (left) and `NO ADF` (right) option. Canbakan 2 level scheme with SPH equivalence.

has been executed considering their implementation separately. We remarked that regarding the pin power reconstruction, massive discrepancies over 30% of are observed when CDF and GFF are not recovered from the lattice calculation. For this reason, the activation of CDF and GFF is surely recommended to maintain the accuracy of the reconstruction. It should also be remarked that in the case of the *DRAGOR-V1 1lvl* scheme, a volume correction has been applied following the pin power reconstruction, to take into account the dilution of the GFF in the outer row of the assembly due to the inclusion of the water gap in the pin mesh.

### *D. Environmental effect*

This work represents a preliminary study for the implementation of a calculation scheme between DRAGON5-PARCS and we did not investigate any improvements respect the single assembly calculation performed with DRAGON5. The environmental effect is not taken into account, and it can be addressed as the primary source of inaccuracies, particularly for the MOX-UOX interface[20]. Several studies have demonstrated the need for performing corrections to this model to mitigate the significant discrepancies that arise in case of heterogeneous configurations[19][21][22][23][24]. The main suggestion is to maintain the single assembly framework but to implement a re-homogenization procedure to account for the spatial and spectral effects of the environment.

## V. CONCLUSIONS

A calculation scheme has been implemented between the lattice code DRAGON5 and the nodal code PARCS, and the pin power reconstruction has been tested. Five lattice schemes have been studied, and a reactor database containing the homogenized parameters have been created to perform the diffusion calculation. The scheme DRAGON5-PARCS has been examined on a 3x3 cluster, and the results have been validated with a stochastic calculation using SERPENT2.

The first part has been dedicated on the validation of the lattice scheme used to generate the homogenized parameters required for the nodal calculation. These calculations have been performed on a single assembly in infinite lattice approximation considering different leakage models. A comparison of the lattice schemes currently adopted by EPM and IRSN was shown, and a preliminary investigation of the sources of discrepancies have been conducted respect to a Monte Carlo reference.

The second part of the work has been focused on the val-

idation of the diffusion calculation performed with PARCS and the analysis of the influence of the leakage model and the methodology to compute ADF on the nodal solution and the pin power reconstruction process. The diffusion calculations have been executed on a simplified core configuration to treat issues where the environmental effects are particularly enhanced. Some limitations of the implemented model derive from the infinite-medium approximation used to perform the lattice calculation.

A net impact of the use of ADF has been observed concerning the assembly power map and the reactivity. Furthermore, the positive influence of the ADFs has been assessed for the reconstruction process. The magnitude of the improvement vary for each particular case, as shown in the comparison between the UA-UOX and the MOX-UOX cluster configurations.

Regarding the leakage model, the $P_1$ approximation has shown slightly worst result than the $B_1$ option, and the latter is recommended. Even if it may presents better results in some particular case, the calculation without leakage model has not been considered due to its applicability in a practical reactor.

In conclusion, the Canbakan 2 level scheme with SPH using the `FD_B` option seems the overall best alternative to generating proper reactor database for nodal diffusion calculations. On the other side, the *DRAGOR-V1 1lvl* scheme does not present sufficient accuracy to be adopted in combination with this core calculation method.

The result of this work is consistent with what has been observed in several previous studies. This is a preliminary investigation and important test for the implementation of an efficient calculation scheme between DRAGON5 and PARCS. The primary sources of error have been analyzed and will be addressed for future improvements of the model.

## VI. ACKNOWLEDGMENTS

The authors would like to thank US/NRC for providing the PARCS computer tool and user support.

## APPENDIX

The tables containing the results of the implementation of the $P_1$ homogeneous model are presented hereafter.

## REFERENCES

1. S. PIGNET ET AL., "The IRSN Orion project: development of new capabilities for neutronics deterministic simulations dedicated to safety analysis," .
2. A. HÉBERT, "DRAGON5 and DONJON5, the contribution of École Polytechnique de Montréal to the SALOME platform," *Annals of Nuclear Energy*, **87, Part 1**, 12–20 (2016).
3. T. DOWNAR ET AL., "PARCS v2. 6 US NRC core neutronics simulator theory manual," *Purdue University/NRC* (2004).
4. K. S. SMITH, "Assembly homogenization techniques for light water reactor analysis," *Progress in Nuclear Energy*, **17**, *3*, 303–335 (1986).
5. R. SANCHEZ, "Assembly homogenization techniques for core calculations," *Progress in Nuclear Energy*, **51**, *1*, 14–31 (2009).
6. R. M. J. VALLERENT, *Développement et validation de schémas de calcul à double niveau pour les réacteurs à eau sous pression*, Master's thesis, École Polytechnique de Montréal (Canada (2009).
7. A. CANBAKAN and A. HEBERT, "Accuracy of a 2-level scheme based on a subgroup method for pressurized water reactor fuel assembly models," *Annals of Nuclear Energy*, **81**, 164–173 (2015).
8. A. H. G. MARLEAU and R. ROY, "A USER GUIDE FOR DRAGON VERSION5," Tech. Rep. IGE-349, École Polytechnique de Montréal (Canada (2015).
9. R. CHAMBON, "Implementation of pin power reconstruction capabilities in the DRAGON5/PARCS system," Tech. Rep. IGE-349, École Polytechnique de Montréal (Canada (2015).
10. J. LEPPÄNEN, M. PUSA, T. VIITANEN, V. VALTAVIRTA, and T. KALTIAISENAHO, "The Serpent Monte Carlo code: Status, development and applications in 2013," *Annals of Nuclear Energy*, **82**, 142–150 (2015).
11. T. DOWNAR, D. LEE, Y. XU, and T. KOZLOWSKI, "Theory manual for the PARCS neutronics core simulator," *School of Nuclear Engineering, Purdue University, W. Lafayette, Indiana*, **47907** (2004).
12. J. VIDAL ET AL., "New modelling of LWR assemblies using the APOLLO2 code package," *Proc. Joint Int. Top. Mtg. on Mathematics & Computation and Supercomputing in Nuclear Applications (M&C+ SNA 2007)*, pp. 15–19 (2007).
13. A. SANTAMARINA, C. COLLIGNON, and C. GARAT, "French calculation schemes for light water reactor analysis," *The Physics of Fuel Cycles and Advanced Nuclear Systems: Global Developments (PHYSOR 2004)* (2004).
14. A. CANBAKAN, *Validation d'un nouveau calcul de référence en évolution pour les réacteurs thermiques*, Master's thesis, École Polytechnique de Montréal (Canada (2014).
15. A. HÉBERT, "Development of the subgroup projection method for resonance self-shielding calculations," *Nuclear science and engineering*, **162**, *1*, 56–75 (2009).
16. A. HÉBERT, *Applied reactor physics*, Presses internationales Polytechnique, Montréal, 2 ed. (2016).
17. R. J. STAMM'LER and M. J. ABBATE, *Methods of steady-state reactor physics in nuclear design*, vol. 111.
18. Y. XU and T. DOWNAR, "GenPMAXS code for generating the PARCS cross section interface file PMAXS," *Purdue University, School of Nuclear Engineering, West Lafayette, IN, USA* (2006).
19. K. SMITH, "Nodal diffusion methods: Understanding numerous unpublished details," in "Proc. Int. Conf. PHYSOR," (2016).
20. T. DOWNAR, C. LEE, and G. JIANG, "An assessment of advanced nodal methods for MOX fuel analysis in light water reactors," in "Proceedings of the PHYSOR 2000 ANS International Topical Meeting on Advances in Reactor Physics and Mathematics and Computation into the Next Millennium. Pittsburgh, Pennsylvania," (2000).

| | UA-UOX | | | | | | MOX-UOX | | | | | |
|---|---|---|---|---|---|---|---|---|---|---|---|---|
| | FD_B | | FD_H | | NO ADF | | FD_B | | FD_H | | NO ADF | |
| | $k_{eff}$ | $\Delta\rho$ | $k_{eff}$ | $\Delta\rho$ | $k_{eff}$ | $\Delta\rho$ | $k_{eff}$ | $\Delta\rho$ | $k_{eff}$ | $\Delta\rho$ | $k_{eff}$ | $\Delta\rho$ |
| *Canb 2lvl SPH* | 1.33600 | -360 | 1.33573 | -375 | 1.33327 | -513 | 1.35282 | -255 | 1.35256 | -270 | 1.35253 | -271 |
| *Canb 2lvl w/o SPH* | 1.33360 | -494 | 1.33333 | -510 | 1.33084 | -650 | 1.35067 | -373 | 1.35041 | -387 | 1.35038 | -389 |
| *Canb 1lvl* | 1.33770 | -265 | 1.33741 | -281 | 1.33493 | -420 | 1.35475 | -150 | 1.35447 | -165 | 1.35444 | -167 |
| *Vall WM 2lvl* | 1.33578 | -372 | 1.33550 | -388 | 1.33300 | -528 | 1.35245 | -275 | 1.35219 | -290 | 1.35217 | -291 |
| *DRAGOR-V1 1lvl* | 1.33937 | -171 | 1.33937 | -172 | 1.33722 | -291 | 1.35723 | -15 | 1.35704 | -26 | 1.35705 | -25 |

TABLE VIII. $k_{eff}$ and reactivitiy [*pcm*] for the motif UA-UOX (Reference SERPENT2 $k_{eff}$ = 1.34245) and MOX-UOX (Reference ERPENT2: $k_{eff}$ = 1.35751). $P_1$ homogeneous leakage model.

| | UA-UOX | | | | | | | | | MOX-UOX | | | | | | | | |
|---|---|---|---|---|---|---|---|---|---|---|---|---|---|---|---|---|---|---|
| | FD_B | | | FD_H | | | NO ADF | | | FD_B | | | FD_H | | | NO ADF | | |
| | Crn | Ctr | Side | Crn | Ctr | Side | Crn | Ctr | Side | Crn | Ctr | Side | Crn | Ctr | Side | Crn | Ctr | Side |
| *Canb 2lvl SPH* | -0.38 | 2.86 | 0.01 | -0.39 | 3.67 | -0.10 | -0.40 | 11.22 | -1.15 | -0.83 | 4.65 | -0.05 | -0.87 | 6.85 | -0.46 | -0.83 | 7.96 | -0.72 |
| *Canb 2lvl w/o SPH* | -0.33 | 2.40 | 0.02 | -0.33 | 3.21 | -0.09 | -0.34 | 10.81 | -1.15 | -0.84 | 4.69 | -0.05 | -0.87 | 6.89 | -0.46 | -0.84 | 8.01 | -0.72 |
| *Canb 1lvl* | -0.42 | 3.02 | 0.03 | -0.43 | 3.86 | -0.08 | -0.44 | 11.46 | -1.14 | -0.89 | 4.92 | -0.04 | -0.93 | 7.23 | -0.46 | -0.89 | 8.33 | -0.73 |
| *Vall WM 2lvl* | -0.38 | 2.76 | 0.02 | -0.39 | 3.58 | -0.08 | -0.40 | 11.23 | -1.15 | -0.83 | 4.69 | -0.06 | -0.86 | 6.88 | -0.47 | -0.82 | 7.96 | -0.73 |
| *DRAGOR-V1 1lvl* | -0.29 | 3.44 | -0.17 | -0.28 | 3.49 | -0.19 | -0.27 | 9.90 | -1.10 | -0.80 | 5.44 | -0.24 | -0.84 | 6.77 | -0.47 | -0.80 | 7.61 | -0.68 |

TABLE IX. Assembly Power (% difference) for the motif UA-UOX and MOX-UOX. $P_1$ homogeneous leakage model. Crn=corner ssembly, Ctr=Center Assembly and Side=Side Assembly

| | FD_B | | | | FD_H | | | | NO ADF | | | |
|---|---|---|---|---|---|---|---|---|---|---|---|---|
| | max | min | rms | $\delta$ | max | min | rms | $\delta$ | max | min | rms | $\delta$ |
| *Canb 2lvl SPH* | 2.28 | -3.21 | 0.62 | 5.49 | 1.33 | -3.65 | 0.65 | 4.97 | 6.96 | -14.04 | 2.95 | 20.99 |
| *Canb 2lvl w/o SPH* | 2.65 | -3.18 | 0.59 | 5.83 | 1.73 | -3.04 | 0.56 | 4.76 | 7.05 | -13.85 | 2.83 | 20.90 |
| *Canb 1lvl* | 2.27 | -3.44 | 0.66 | 5.71 | 1.44 | -3.88 | 0.72 | 5.33 | 6.71 | -14.15 | 3.01 | 20.86 |
| *Vall WM 2lvl* | 2.37 | -3.21 | 0.61 | 5.58 | 1.42 | -3.59 | 0.64 | 5.00 | 6.91 | -14.07 | 2.95 | 20.99 |
| *DRAGOR-V1 1lvl* | 2.97 | -7.32 | 1.06 | 10.28 | 2.70 | -7.26 | 1.05 | 9.95 | 7.15 | -11.70 | 2.86 | 18.85 |

TABLE X. Pin Power (% difference) for the colorset UA-UOX. $P_1$ homogeneous leakage model.

| | FD_B | | | | FD_H | | | | NO ADF | | | |
|---|---|---|---|---|---|---|---|---|---|---|---|---|
| | max | min | rms | $\delta$ | max | min | rms | $\delta$ | max | min | rms | $\delta$ |
| *Canb 2lvl SPH* | 2.17 | -9.35 | 2.25 | 11.52 | 2.55 | -11.25 | 2.56 | 13.80 | 4.05 | -12.25 | 2.81 | 16.29 |
| *Canb 2lvl w/o SPH* | 2.12 | -9.45 | 2.27 | 11.56 | 2.45 | -11.25 | 2.58 | 13.70 | 4.01 | -12.26 | 2.82 | 16.26 |
| *Canb 1lvl* | 1.96 | -9.80 | 2.36 | 11.76 | 2.50 | -11.51 | 2.70 | 14.01 | 3.74 | -12.50 | 2.93 | 16.24 |
| *Vall WM 2lvl* | 2.12 | -9.38 | 2.25 | 11.50 | 2.57 | -11.23 | 2.57 | 13.80 | 4.10 | -12.18 | 2.80 | 16.28 |
| *DRAGOR-V1 1lvl* | 2.61 | -9.72 | 2.29 | 12.33 | 2.63 | -10.73 | 2.58 | 13.36 | 3.96 | -11.23 | 2.75 | 15.19 |

TABLE XI. Pin Power (% difference) for the colorset MOX-UOX. $P_1$ homogeneous leakage model.

21. K. S. SMITH, "Practical and efficient iterative method for LWR fuel assembly homogenization," *Transactions of the American Nuclear Society*, **71**, *CONF-941102–* (1994).
22. F. RAHNEMA and E. M. NICHITA, "Leakage corrected spatial (assembly) homogenization technique," *Annals of Nuclear Energy*, **24**, *6*, 477–488 (1997).
23. S. PALMTAG and K. SMITH, "Two-group spectral corrections for MOX calculations," in "Proc. Int. Conf. Physics of Nucl. Sci. and Tech," (1998), vol. 1, p. 3.
24. A. DALL'OSSO, "Spatial rehomogenization of cross sections and discontinuity factors for nodal calculations," in "Proc. of Int. Conf. PHYSOR," (2014).